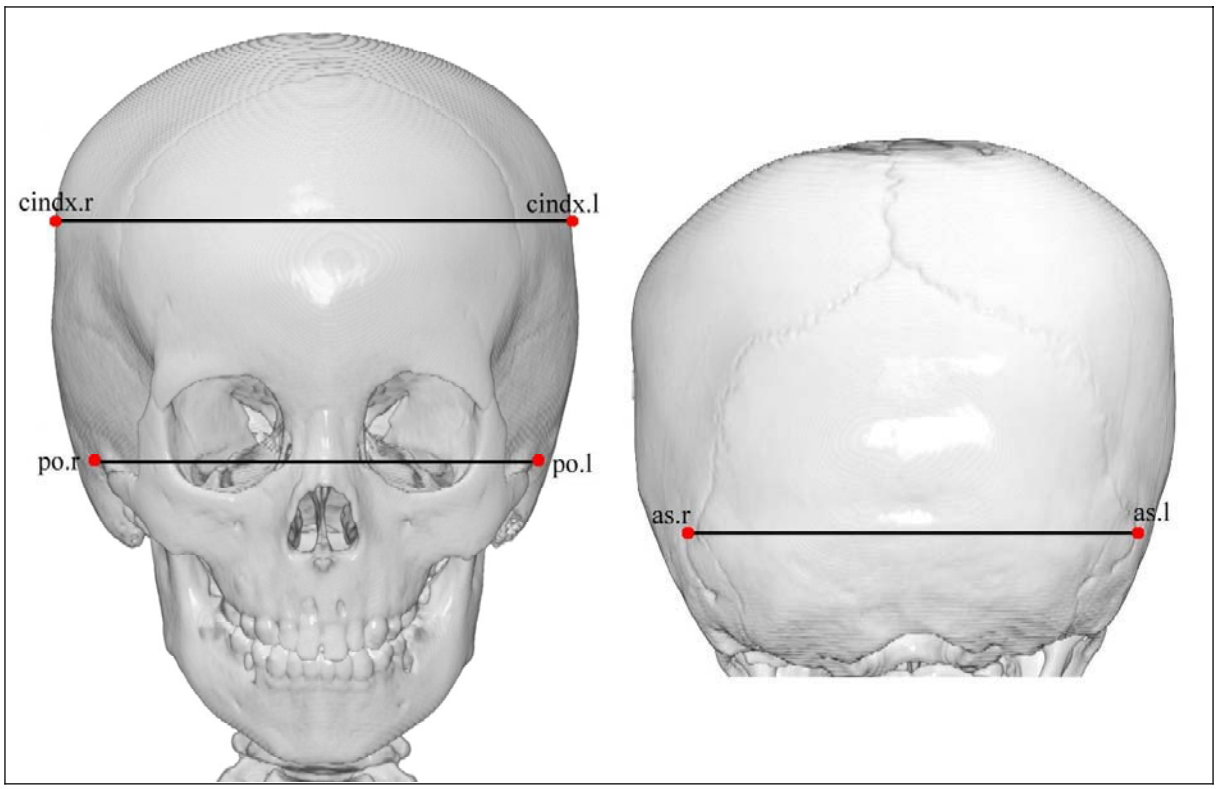

Figure 2.7 3D-CT of the skull in frontal and posterior views showing measurements for cranial vault width

Cranial vault width

cindx.l-cindx.r	Maximum cranial width
as.l-as.r	Interasterion width
po.l-po.r	Interporion width

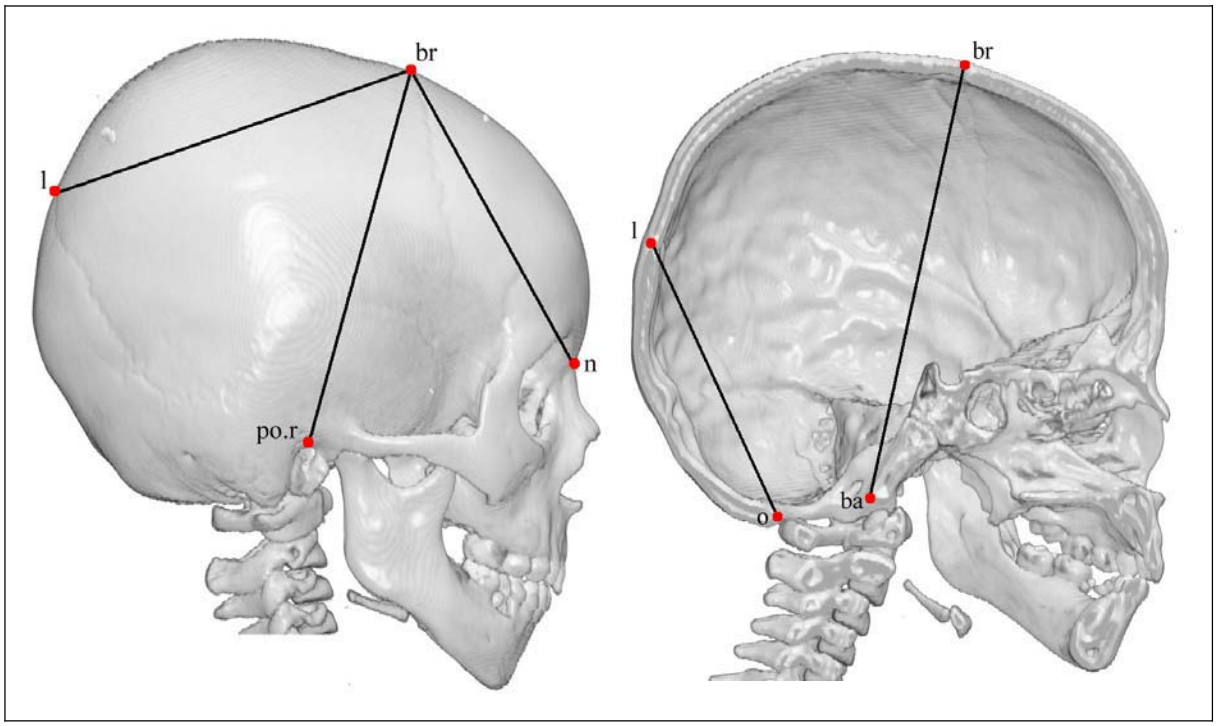

Figure 2.8 3D-CT of the skull in lateral and mid-sagittal views showing measurements for cranial vault height.

Cranial vault height

ba-br	Cranial height
br-po.l	Left lateral cranial vault height
br-po.r	Right lateral cranial vault height
n-br	Anterior cranial vault height
l-br	Posterior cranial vault height
l-o	Lambdoid height

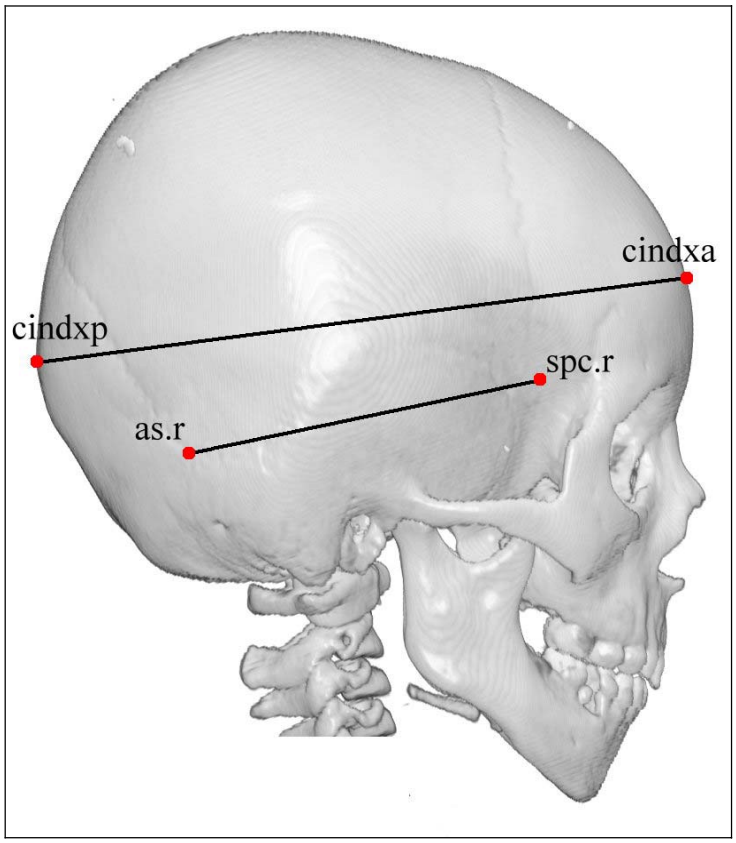

Figure 2.9 3D-CT of the skull in lateral view showing measurements for cranial vault length.

Cranial vault length

cindxa-cindxp	Maximum cranial length
spc.l-as.l	Left cranial vault length
spc.r-as.r	Right cranial vault length

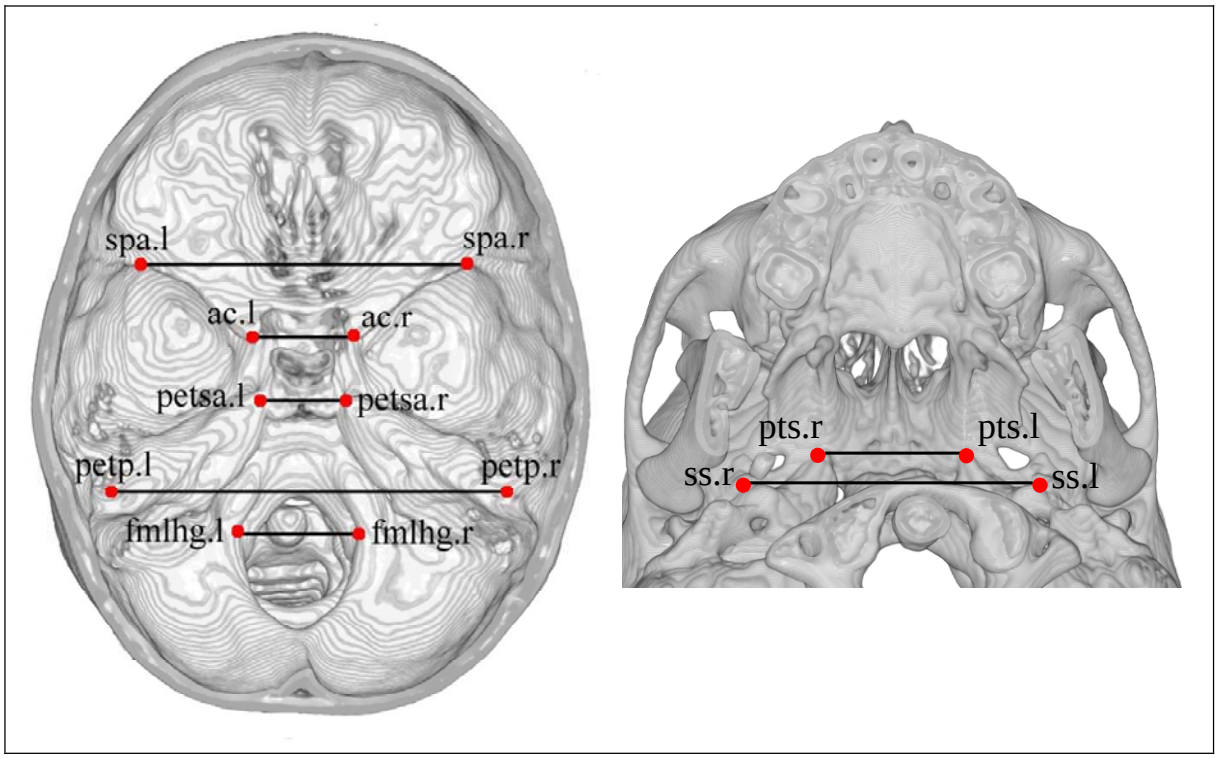

Figure 2.10 3D-CT of the cranial base from superior and inferior views showing measurements for cranial base width.

Cranial base width

spa.l-spa.r	Anterior cranial base width
ac.l-ac.r	Anterior clinoid distance
petsa.l-petsa.r	Superior spheno-occipital synchondrosis width
pts.l-pts.r	Inferior spheno-occipital synchondrosis width
petp.l-petp.r	Posterior cranial fossa width
ss.l-ss.r	External cranial base width
fmlhg.l-fmlhg.r	Foramen magnum width

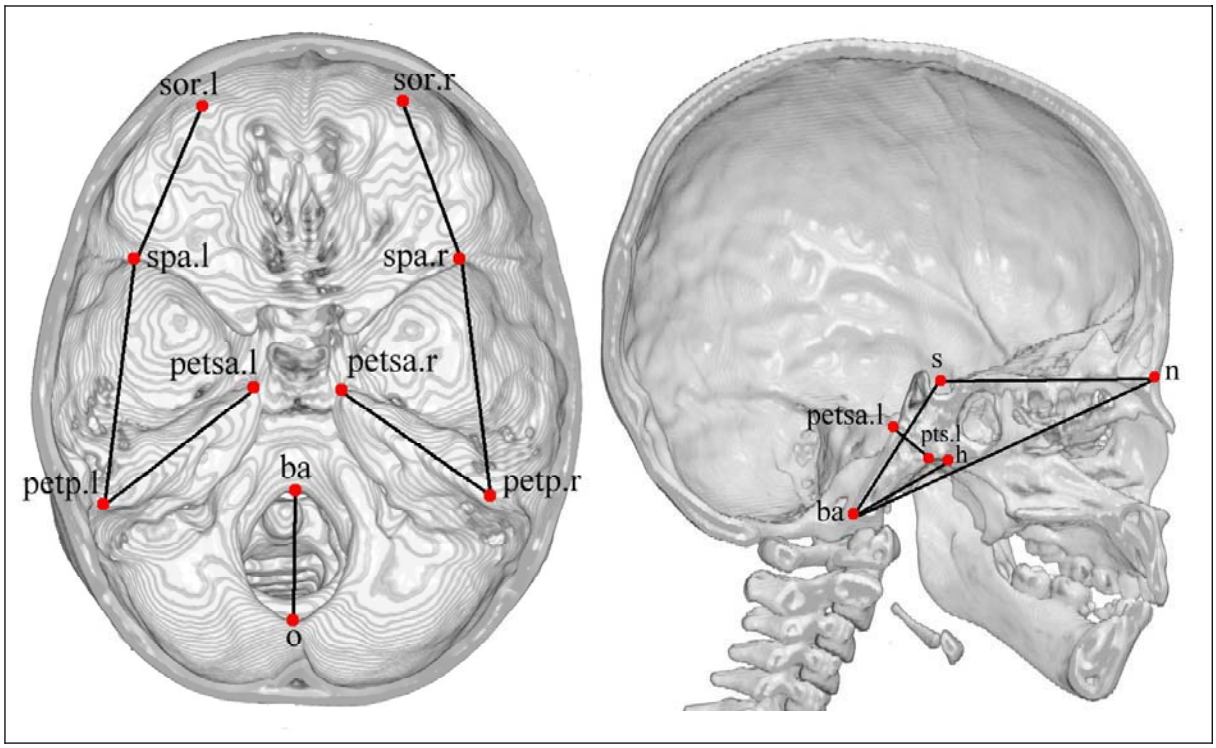

Figure 2.11 3D-CT of the cranial base from superior and mid-sagittal views showing measurements for cranial base length.

Cranial base length

sor.l- spa.l	Left anterior cranial fossa length
sor.r- spa.r	Right anterior cranial fossa length
spa.l-petp.l	Left lateral middle cranial fossa length
spa.r-petp.r	Right lateral middle cranial fossa length
petsa.l-petp.l	Left petrous ridge length
petsa.r-petp.r	Right petrous ridge length
pts.l-petsa.l	Left spheno-occipital synchondrosis length
pts.r- petsa.r	Right spheno-occipital synchondrosis length
ba-o	Foramen magnum length
ba-h	Inferior posterior cranial base length
ba-n	Cranial base length
s-n	Anterior cranial base length
ba-s	Posterior cranial base length

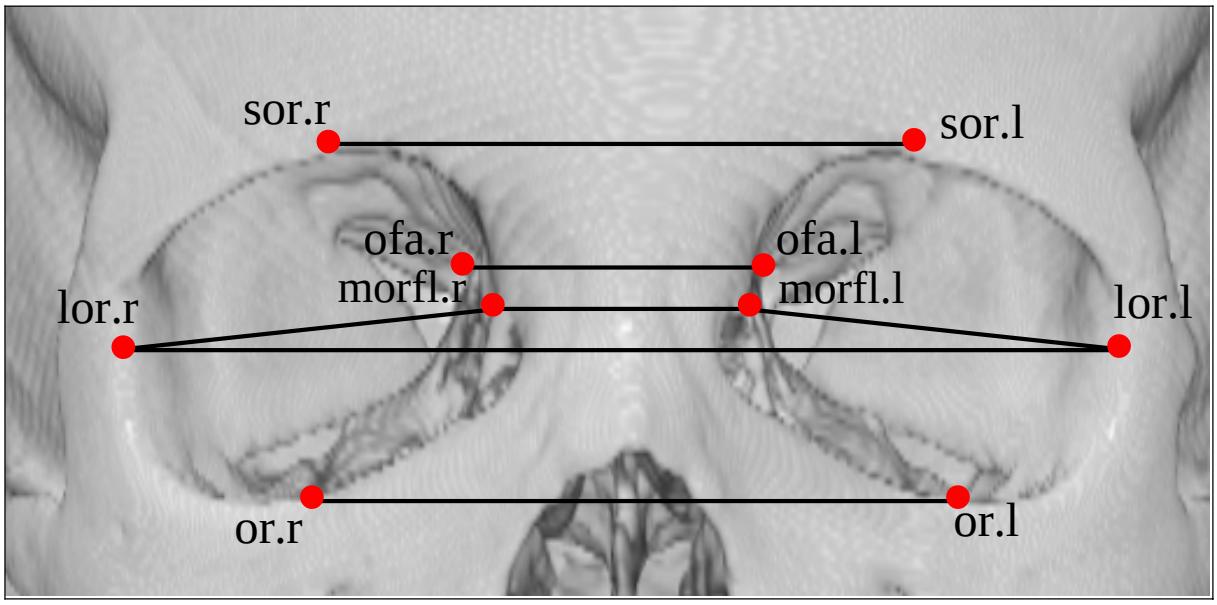

Figure 2.12 3D-CT of the orbit showing measurements for orbital width.

Orbital width

sor.l-sor.r	Anterior superior orbital width
morfl.l-morfl.r	Interorbital width
lor.l-lor.r	Maximum orbital width
or.l-or.r	Anterior inferior orbital width
ofa.l-ofa.r	Posterior orbital width
lor.l-morfl.l	Left orbital distance
lor.r-morfl.r	Right orbital distance

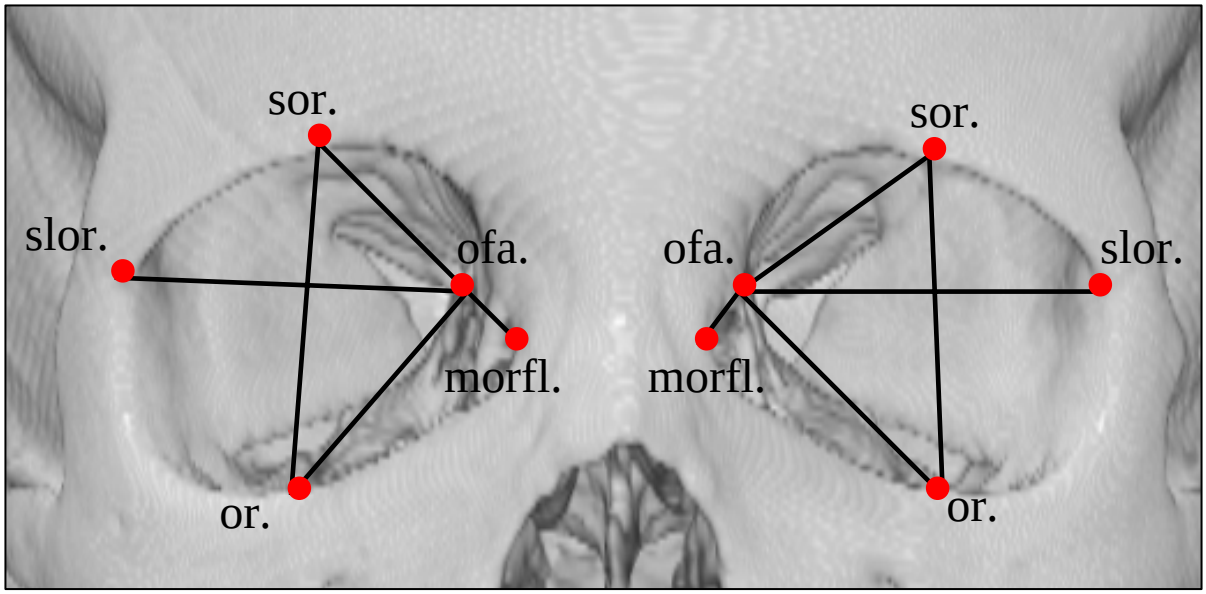

Figure 2.13 3D-CT of the orbit showing measurements for orbital height and length.

Orbital height

sor.l-or.l	Left orbital height
sor.r-or.r	Right orbital height

Orbital length

ofa.l-sor.l	Left superior orbital length
ofa.r-sor.r	Right superior orbital length
ofa.l-or.l	Left inferior orbital length
ofa.r-or.r	Right inferior orbital length
ofa.l-morfl.l	Left medial orbital length
ofa.r-morfl.r	Right medial orbital length
ofa.l-slor.l	Left lateral orbital length
ofa.r-slor.r	Right lateral orbital length

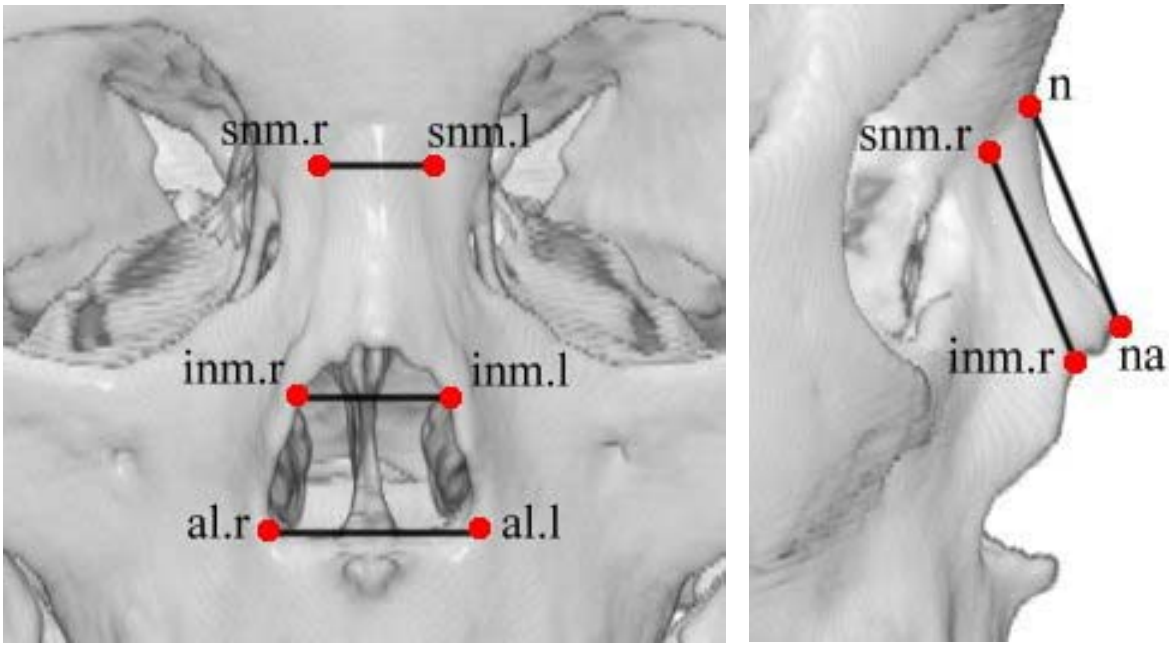

Figure 2.14 3D-CT of the nasal bone showing measurements for nasal width and length.

Nasal width

snm.l-snm.r	Superior nasal width
inm.l-inm.r	Inferior nasal width
al.l-al.r	Nasal aperture width

Nasal length

inm.l-snm.l	Left naso-maxillary suture length
inm.r-snm.r	Right naso-maxillary suture length
na-n	Nasal bone length

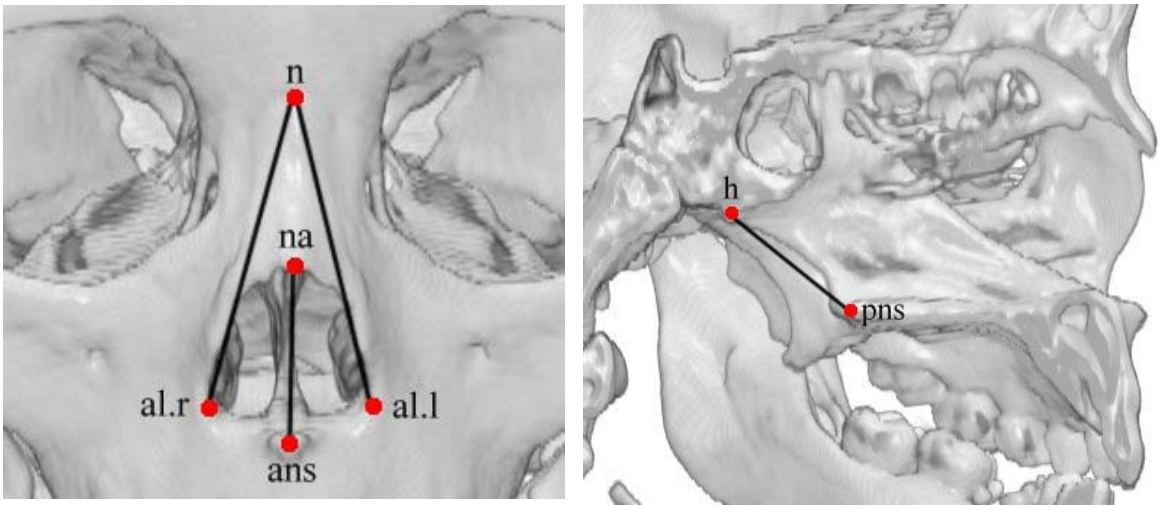

Figure 2.15 3D-CT of the nasal bone showing measurements for nasal height.

Nasal height

n-al.l	Left nasal height
n-al.r	Right nasal height
na-ans	Nasal aperture height
pns-h	Posterior nasal height

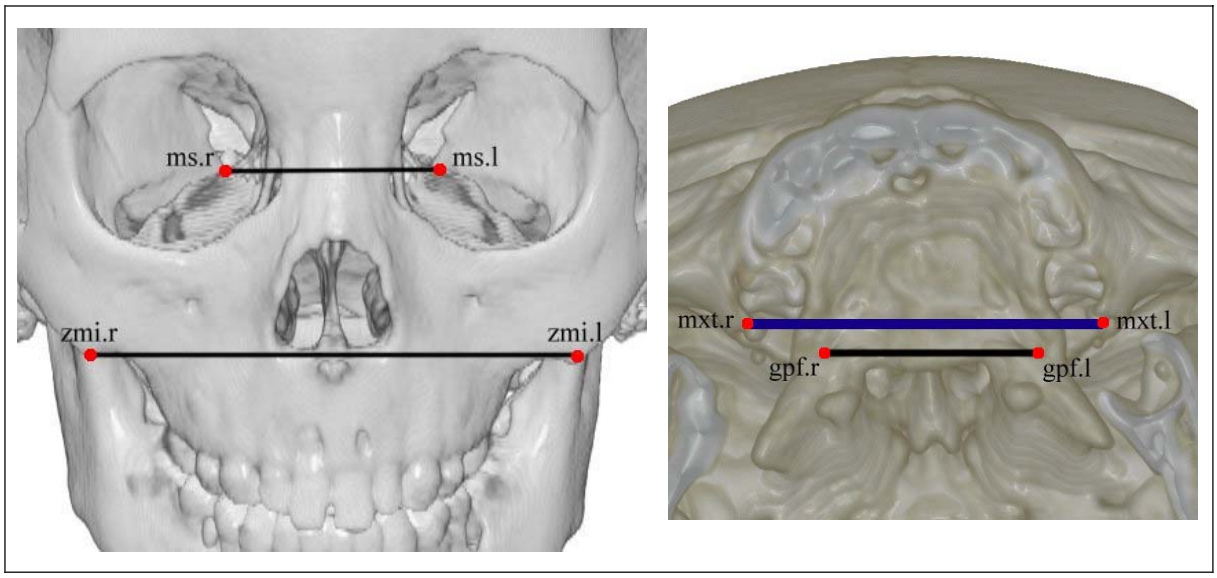

Figure 2.16 3D-CT of the maxilla showing measurements for maxillary width.

Maxillary width

zmi.l-zmi.r	Maximum maxillary width
ms.l-ms.r	Posterior superior maxillary width
mxt.l-mxt.r	Posterior inferior maxillary width
gpf.l-gpf.r	Posterior palatal width

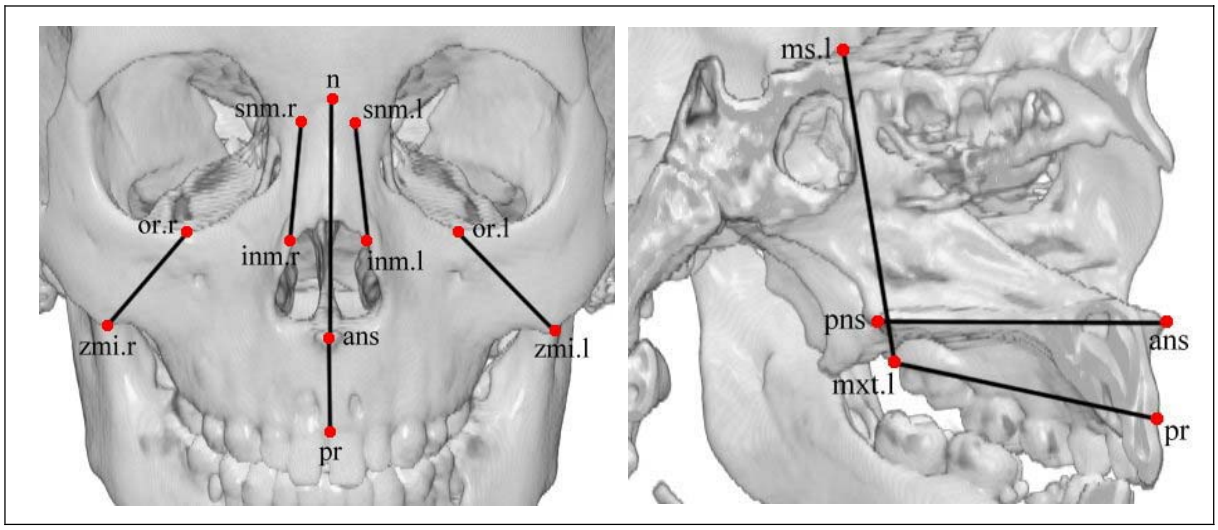

Figure 2.17 3D-CT of the maxilla showing measurements for maxillary height and length.

Maxillary height

n-ans	Anterior upper face height
ans-pr	Anterior maxillary alveolar height
mxt.l-ms.l	Left posterior maxillary height
mxt.r-ms.r	Right posterior maxillary height

Maxillary length

or.l-zmi.l	Left anterior zygo-maxillary suture length
or.r-zmi.r	Right anterior zygo-maxillary suture length
inm.l-snm.l	Left naso-maxillary suture length
inm.r-snm.r	Right naso-maxillary suture length
mxt.l-pr	Left inferior maxillary length
mxt.r-pr	Right inferior maxillary length
pns-ans	Palatal length

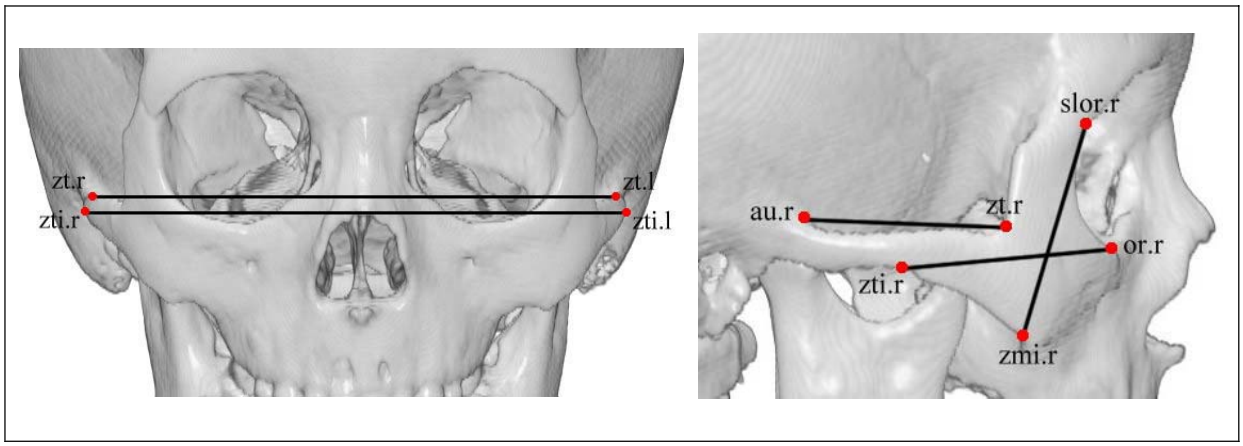

Figure 2.18 3D-CT of the zygoma showing measurements for zygomatic width, height and length.

Zygomatic width

zt.l-zt.r	Superior zygomatic width
zti.l-zti.l	Inferior zygomatic width

Zygomatic height

slor.l-zmi.l	Left zygomatic height
slor.r-zmi.r	Right zygomatic height

Zygomatic length

zt.l-au.l	Left zygomatic arch length
zt.r-au.r	Right zygomatic arch length
zti.l-or.l	Left zygomatic length
zti.r-or.r	Right zygomatic length

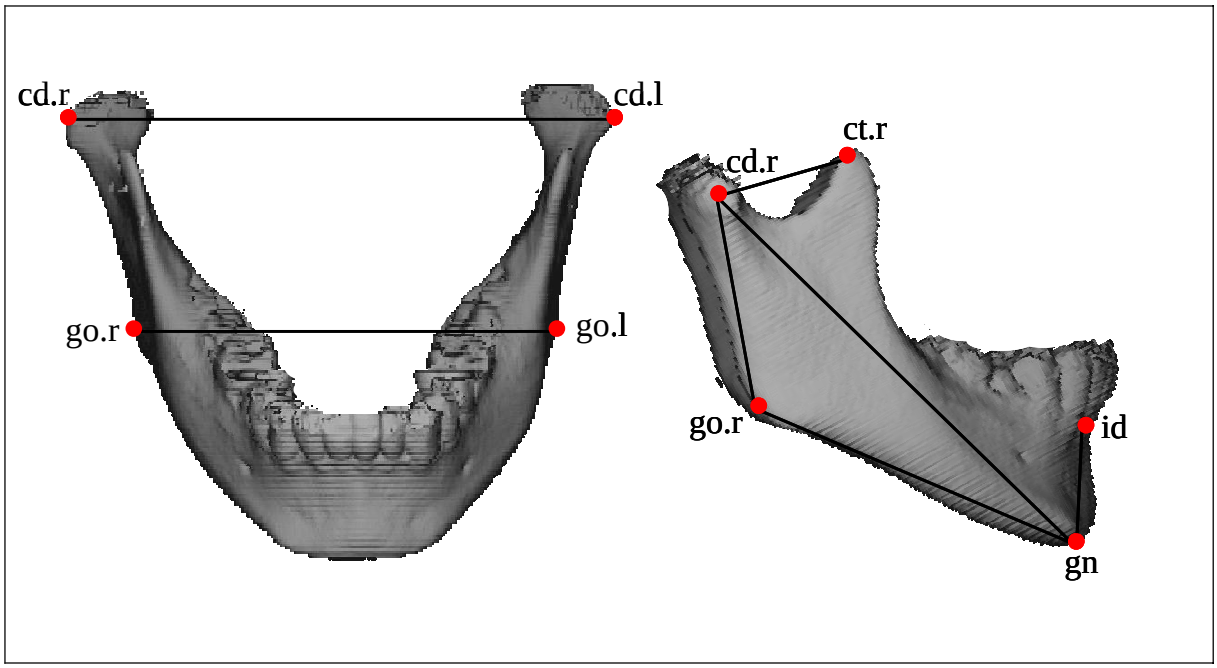

Figure 2.19 3D-CT of the mandible showing measurements for mandibular width, height and length.

Mandibular width

go.l-go.r	Intergonial width
cd.l-cd.r	Intercondylar width
cd.l-ct.l	Left superior ramus width
cd.r-ct.r	Right superior ramus width

Mandibular height

cd.l-go.l	Left ramus height
cd.r-go.r	Right ramus height
gn-id	Anterior mandibular alveolar height

Mandibular length

go.l-gn	Left mandibular body length
go.r-gn	Right mandibular body length
gn-cd.l	Left total mandibular length
gn-cd.r	Right total mandibular length

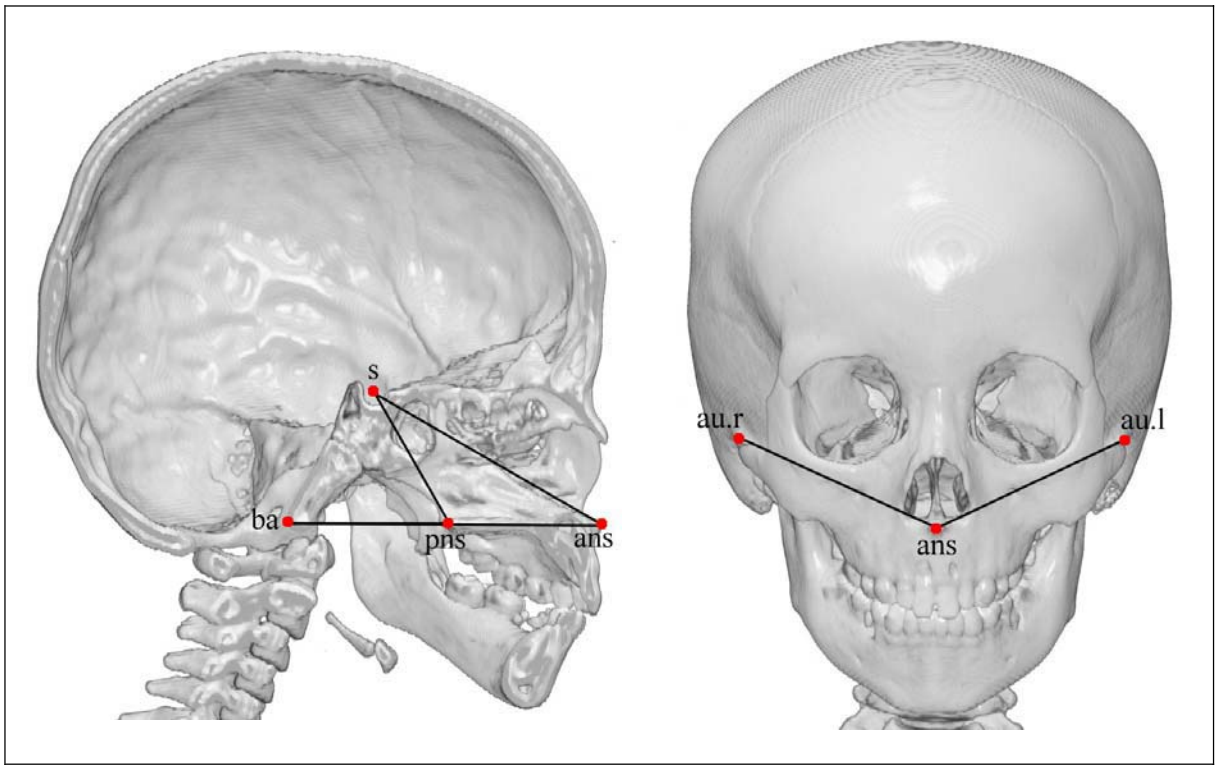

Figure 2.20 3D-CT of the skull showing measurements for inter-regional regions.

Inter-regional variables

s-pns

s-ans

ba-pns

ba-ans

au.l-ans Left total face length

au.r-ans Right total face length

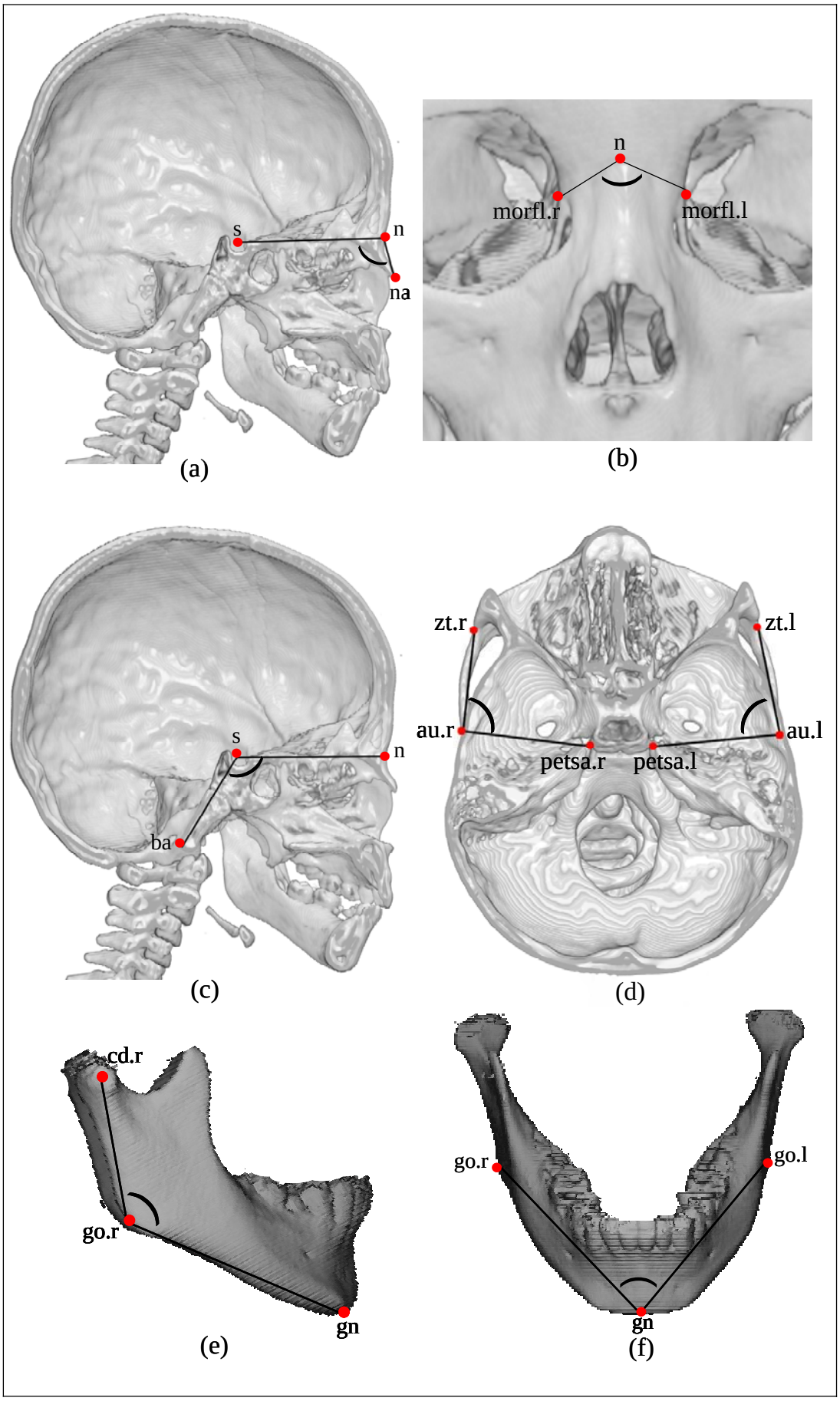

Figure 2.21 3D-CT images (a) to (j) showing angular measurements.

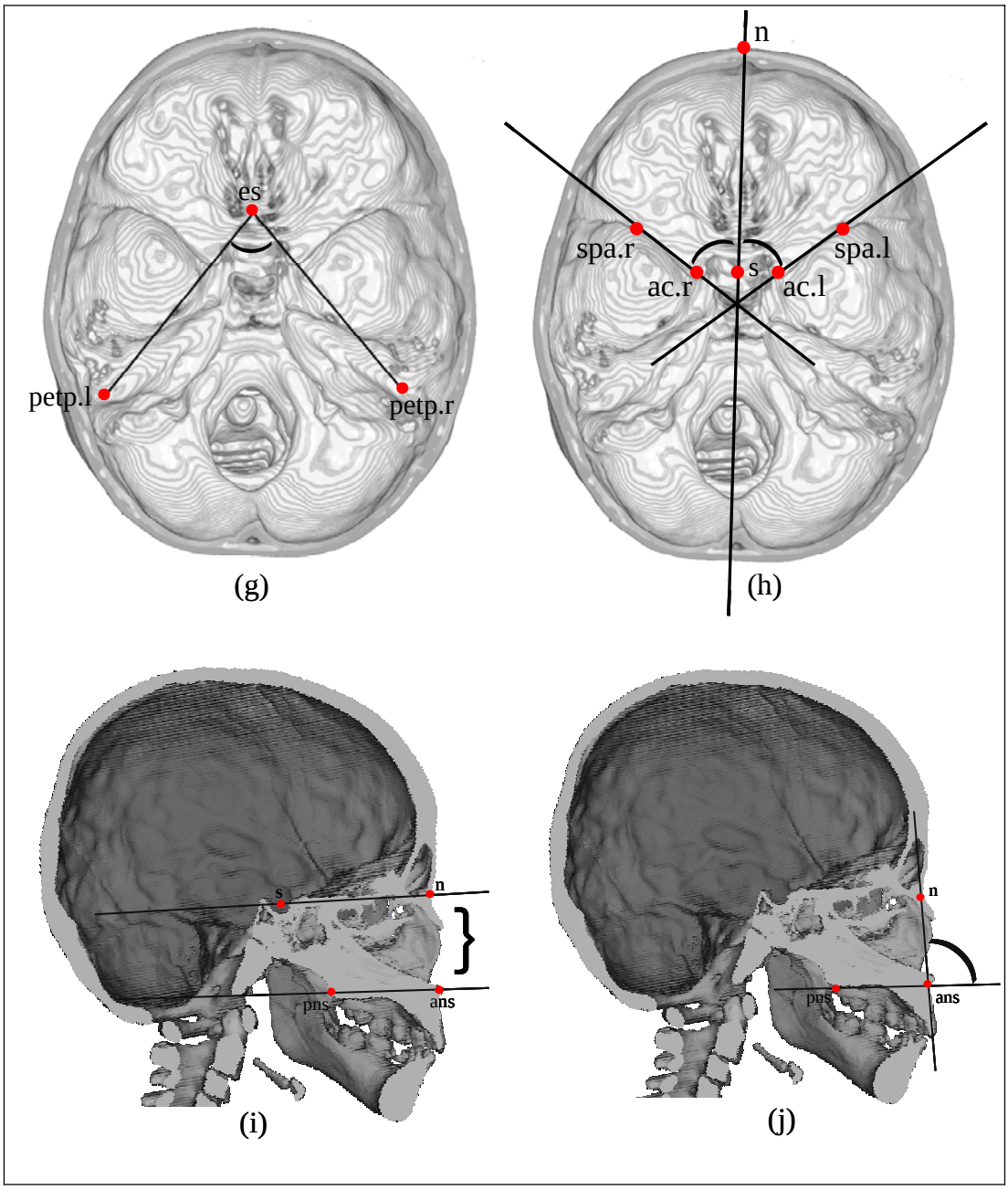

Figure 2.21 (cont.)

Angular measurements

s-n-na	Nasal angle relative to anterior cranial base
morfl.l-n-morfl.r	Interorbital angle
ba-s-n	Midline cranial base angle
petsa.l-au.l-zt.l	Left zygoma projection angle

petsa.r-au.r-zt.r	Right zygoma projection angle
cd.l-go.l-gn	Left gonial angle
cd.r-go.r-gn	Right gonial angle
go.l-gn-go.r	Anterior mandibular angle
petp.l-es-petp.r	Petrous posterius anterior angle
s-n/ac.l-spa.l	Left lateral projection of lesser wing
s-n/ac.r-spa.r	Right lateral projection of lesser wing
s-n/ans-pns	Palatal plane relative to anterior cranial base angle
n-ans/ans-pns	Palatal plane/face height angle

Indices/Ratio

cindx.l-cindx.r:cindxa-cindxp	Cephalic index
sor.l-or.l:morfl.l-lor.l	Left orbital index
sor.r-or.r :morfl.r-lor.r	Right orbital index

2.7 Overview of Statistical Analysis of Measurement Techniques

A series of statistical analyses was performed on the collected data for different purposes. More detailed descriptions of these analyses will be provided in subsequent chapters. In Chapter 3, which mainly concerns with generation of new reference data for craniofacial measurements, descriptive statistics such as mean values, standard deviations, standard errors and coefficients of variation are presented. Scatter plots of variables against age are also presented in this chapter and non-linear regression (growth) curves serve as graphical presentations.

A linear modelling approach was used to compare mean values between males and females. This method was used instead of a t-test because the ages of the males and females in the various age categories were not matched exactly for comparison. Linear modelling allowed comparisons to be made of adjusted mean ages in each of the selected age categories.

Paired t-tests were used to compare values between left and right sides for selected variables. A linear modelling approach was also applied and plots generated to provide graphical presentations of asymmetry.

Finally, Student's t-test was utilised to compare the mean values of some of the measurements from the Malay sample with published data from two studies of other ethnic groups at selected ages.

2.8 Error of Measurements and Analysis

In this type of study where measurements are involved, it is important to establish the degree of reliability of methods adopted. Researchers need to take into account the errors of observation arising from the technique applied when making comparisons within and between groups. Additionally, it is important to differentiate between the basic terms of validity and reproducibility before exploring errors of measurements.

Validity refers to how well an instrument measures what it is supposed to measure in the absence of measurement error. The term accuracy may also be used in this context.

Reproducibility or reliability means the closeness of successive measurements of the same object. Reproducibility is affected by the condition of the object being measured, the quality of records, the situation in which measurements are made, and the care and skill of the measurer.

2.8.1 Type of Errors

There are two types of measurement errors i.e. systematic and random errors. Systematic errors (or bias) occur if a particular measurement is persistently over- or under-recorded. Examples of how systematic errors can occur include measurements being made by different persons who have different concepts of a particular landmark, or when an observer's practice changes with experience over a period of time (Houston, 1983).

In cephalometry, random errors can arise from variations in positioning of subjects in the cephalostat during x-ray taking. The greatest source of random errors is difficulty in identifying a particular landmarks or lack of precision in its definition. In view of this, many anatomic definitions lack precision. Despite many attempts being made to improve the

precision of definitions (Van der Linden, 1971), difficulties still exist even when a 3D-CT approach is used.

To determine the landmark relocation error in this project, double determinations were performed for 10% of the subjects. Due to radiation exposure, it was not possible to rescan the patients. Therefore, the double determinations were based on two examinations of the same CT scans performed at least one month apart. This time interval ensured point identification clues would not be recalled to aid in relocation.

2.8.2 Detecting Systematic errors

The simplest approach to detect systematic errors is to conduct a paired t-test to analyse the differences between pairs of determinations. This test calculates whether the mean difference between the two determinations is significantly different from zero.

2.8.3 Calculating Random errors

Random errors may add to the natural variability of the measurements and may therefore obscure real differences between groups. Calculation of the standard deviation of the differences between the two measurements, S_d provides one way of measuring random errors. The variance, S_d^2, of differences between two measures is double that of a single measurement. S_d^2 should therefore be halved to give an estimation of the error of a single measurement.

$$\text{i.e. } S_e^2 = S_d^2/2 \quad \text{therefore} \quad S_e = \sqrt{\frac{\sum d^2}{2N}}$$

This is the formula proposed by Dahlberg (1940) to estimate the standard deviation of a single determination. The term S_e^2 is referred as the error variance.

$$S_e^2 = \Sigma d^2/2n$$

2.8.4 Error Analysis for this Study

Calculation of the error of the method was performed by the process of double determination performed over a specific time interval. Double determinations of different scans of the same subjects would have been more ideal but this was not possible due to ethical objections to unnecessary radiation exposure to the subjects. It would also be more ideal to perform double determinations on all subjects but this was not possible due to the time limitation for this study. Landmarks were determined on the same CT images on two separate occasions for 20 subjects (10%), approximately one month apart. All 115 landmarks were used for the study of reproducibility.

The following provides essentially a multi-variate description of Dahlberg's method of double determination.

The variable of interest (distance measurement or point location) is determined on *n* individuals on two occasions sufficiently separated in time so that non-landmark related cues would be forgotten.

Let $\mathbf{d}_1, \mathbf{d}_2, \ldots, \mathbf{d}_n$ be the observed differences for the *n* double determinations of a *p*-dimensional variable (here 1, 2 or 3 dimensions) and each $\mathbf{d}_j$ have a *p*-variate normal distribution with mean $\boldsymbol{\mu}_d$ and variance-covariance matrix $\boldsymbol{\Sigma}_d$. Then the mean difference vector is given by

$$\bar{\mathbf{d}} = \frac{1}{n}\sum_{j=1}^{n}\mathbf{d}_j$$

and the estimated variance-covariance matrix $\mathbf{S}_d$ is given by (Johnson and Wichern, 1988).

$$\mathbf{S}_d = \frac{1}{n-1}\sum_{j=1}^{n}(\mathbf{d}_j - \bar{\mathbf{d}})(\mathbf{d}_j - \bar{\mathbf{d}})'$$

Bold letters indicate vectors of dimension *p* and the prime indicates transpose.

When the null hypothesis of no systematic error holds $\bar{\mathbf{d}} \sim \mathbf{N}_p(0, \Sigma_d / n)$, that is, $\boldsymbol{\mu}_d = \mathbf{0}$.

The test statistic

$$T^2 = n\bar{\mathbf{d}}'\mathbf{S}_d^{-1}\bar{\mathbf{d}}$$

has a Hotelling's T^2 distribution and is used to test the null hypothesis. The null hypothesis is rejected at the α-level if

$$T^2 > \frac{(n-1)p}{(n-p)} F_{p,n-p}(\alpha)$$

If the null hypothesis is retained then a suitable measure of the variance-covariance matrix of the random error associated with a single determination of a *p*-dimensional variable is:

$$\mathbf{S} = \frac{1}{2n}\sum_{j=1}^{n} \mathbf{d}_j \mathbf{d}_j'$$

The factor of two in the denominator arises because the measurement error can be equally ascribed to either determination. The factor n is used rather than the (*n*-1) because the mean error has been taken to be zero.

In this study $p = 3$ dimensions for point measurements. For anthropometric variables such as distances, where $p = 1$, the formulae reduce to Dahlberg's original formulation of t-tests on the mean differences and assigning the random measurement error, *s*, as

$$s^2 = \frac{1}{2n}\sum_{j=1}^{n} d_j^2$$

In one dimension the T^2 test statistic becomes:

$$T^2 = n\bar{\mathrm{d}}^2 / s_{\mathrm{d}}^2 \sim F_{1,n-1}(\alpha) \quad \text{or} \quad t = T = \sqrt{n}(\bar{\mathrm{d}} / s_{\mathrm{d}}) \sim t_{n-1}(\alpha)$$

where s_d is the estimator of the standard deviation of the differences between each determination and $t_{n-1}(\alpha)$ is Student's t-distribution.

2.8.4.1 Landmark relocation error

Table 2.3 shows the landmark relocation error for all points. The pooled relocation error over 115 landmarks was 0.49mm. The minimum magnitude for landmark relocation error (|**xyz**|) was 0.17mm for pterygo-lateralis left and the maximum magnitude was 1.55mm for petrous posterius left. The median relocation error of 0.40 mm gave an indication of the general relocation error. This error was small and approximately the pixel size of the CT scan (0.488mm).

Some of the landmarks used in the calculation of the error of the method were eventually not used in the measurement analysis. In particular, those landmarks that were not readily identified or not considered to be an essential part of an anatomical unit were excluded.

Table 2.3 Landmark relocation error.

Landmark No	x	y	z	|xyz|	n	Landmark
200	0.28	0.17	0.29	0.44	20	alare left
201	0.38	0.22	0.38	0.58	20	alare right
1000	0.21	0.07	0.19	0.29	19	anterior clinoid left
1001	0.10	0.09	0.22	0.25	19	anterior clinoid right
270	0.18	0.09	0.15	0.25	20	anterior nasal spine
1102	0.22	0.30	0.14	0.40	19	articular fossa left
1103	0.25	0.35	0.15	0.45	20	articular fossa right
800	0.31	0.27	0.24	0.47	19	asterion left
801	0.17	0.23	0.40	0.49	20	asterion right
1104	0.19	0.21	0.24	0.37	19	auriculare left
1105	0.17	0.23	0.23	0.36	20	auriculare right
870	0.24	0.28	0.61	0.71	20	basion
770	0.38	0.44	0.27	0.65	19	bregma
100	0.11	0.28	0.18	0.35	20	condylion laterale left
101	0.08	0.24	0.27	0.37	20	condylion laterale right
102	0.38	0.13	0.52	0.66	20	coronoid base left
103	0.43	0.14	0.70	0.83	19	coronoid base right
104	0.29	0.23	0.15	0.40	20	coronoid tip left
105	0.29	0.32	0.17	0.47	20	coronoid tip right
602	0.17	0.24	0.21	0.36	16	cribriform plate posterius left
603	0.31	0.33	0.26	0.52	17	cribriform plate posterius right
671	0.10	0.16	0.17	0.25	14	ethmoid spine
1114	0.41	0.31	0.14	0.53	19	external auditory meatus superius (ie porion) left
1115	0.26	0.24	0.08	0.36	20	external auditory meatus superius (ie porion) right
672	0.20	0.22	0.35	0.46	15	foramen caecum
1006	0.21	0.20	0.29	0.41	20	foramen out ovale left
1007	0.21	0.17	0.28	0.39	20	foramen out ovale right
170	0.27	0.24	0.09	0.38	18	gnathion
106	0.28	0.19	0.61	0.69	20	gonion left
107	0.36	0.17	0.49	0.64	20	gonion right
224	0.17	0.20	0.25	0.36	20	greater palatine foramen left
225	0.16	0.27	0.28	0.42	20	greater palatine foramen right
1028	0.12	0.30	0.21	0.38	19	greater wing laterale left

Table 2.3 (cont.)

Landmark No	x	y	z	|xyz|	n	Landmark
1029	0.12	0.28	0.23	0.38	19	greater wing laterale right
1010	0.18	0.19	0.08	0.28	19	greater wing mediale left
1011	0.12	0.27	0.12	0.32	19	greater wing mediale right
202	0.22	0.26	0.15	0.37	20	hamular notch left
203	0.32	0.20	0.16	0.41	20	hamular notch right
1012	0.10	0.15	0.13	0.22	20	hamular process left
1013	0.16	0.19	0.20	0.32	19	hamular process right
1070	0.13	0.28	0.24	0.39	20	hormion
204	0.22	0.20	0.21	0.36	20	inferior naso-maxillare left
205	0.27	0.19	0.38	0.51	20	inferior naso-maxillare right
206	0.18	0.34	0.09	0.40	20	inferior orbital fissure left
207	0.21	0.31	0.12	0.40	20	inferior orbital fissure right
171	0.11	0.12	0.17	0.24	19	infradentale
872	0.40	0.25	0.51	0.69	19	lambda
110	0.25	0.28	0.14	0.40	20	mandibular notch left
111	0.19	0.21	0.08	0.29	20	mandibular notch right
1118	0.17	0.18	0.05	0.25	19	mastoidale left
1119	0.21	0.21	0.06	0.30	20	mastoidale right
210	0.40	0.33	0.23	0.57	20	maxillare superius left
211	0.34	0.26	0.23	0.49	20	maxillare superius right
228	0.31	0.18	0.29	0.47	20	maxillary tuberosity left
229	0.31	0.24	0.35	0.52	20	maxillary tuberosity right
271	0.16	0.21	0.16	0.31	20	nasale
272	0.15	0.21	0.28	0.38	19	nasion
214	0.21	0.28	0.13	0.38	20	naso-lacrimal inferius left
215	0.23	0.28	0.12	0.38	20	naso-lacrimal inferius right
874	0.29	0.19	0.30	0.46	20	opisthion
1030	0.23	0.24	0.25	0.41	20	optic foramen a left
1031	0.23	0.31	0.28	0.47	20	optic foramen a right
216	0.52	0.29	0.22	0.64	20	orbitale left
217	0.40	0.24	0.23	0.52	20	orbitale right
1122	0.77	1.01	0.88	1.55	19	petrous posterius left
1123	0.76	0.81	0.69	1.31	20	petrous posterius right
1120	0.26	0.27	0.25	0.45	20	petrous sup-anterius left
1121	0.17	0.12	0.11	0.24	20	petrous sup-anterius right
1018	0.18	0.18	0.18	0.32	20	posterior clinoid left
1019	0.13	0.10	0.07	0.18	20	posterior clinoid right
273	0.19	0.14	0.35	0.42	20	posterior nasal spine
274	0.12	0.17	0.25	0.33	19	prosthion
218	0.10	0.09	0.10	0.17	20	pterygo-lateralis left
219	0.14	0.11	0.23	0.29	20	pterygo-lateralis right
220	0.16	0.15	0.26	0.34	20	pterygo-superius left
221	0.19	0.12	0.21	0.31	20	pterygo-superius right
1071	0.28	0.25	0.32	0.49	20	sella
1022	0.20	0.35	0.34	0.53	18	sphenion c left
1023	0.19	0.38	0.34	0.54	18	sphenion c right
1024	0.22	0.39	0.46	0.64	18	sphenion t left
1025	0.16	0.31	0.44	0.57	19	sphenion t right
1020	0.97	0.43	0.38	1.13	19	sphenoidale anterior left
1021	0.69	0.32	0.50	0.91	20	sphenoidale anterior right
1090	0.14	0.21	0.06	0.26	20	spine of sphenoid left
1091	0.17	0.16	0.06	0.24	20	spine of sphenoid right
1080	0.19	0.11	0.20	0.29	13	sup sphenoid spheno-occipital synchondrosis left
1081	0.23	0.08	0.22	0.33	14	sup sphenoid spheno-occipital synchondrosis right
1082	0.16	0.18	0.17	0.30	13	inf sphenoid spheno-occipital synchondrosis left
1083	0.18	0.14	0.22	0.31	13	inf sphenoid spheno-occipital synchondrosis right
1084	0.22	0.17	0.14	0.32	13	sup occipital spheno-occipital synchondrosis left
1085	0.31	0.20	0.13	0.39	14	sup occipital spheno-occipital synchondrosis right
1086	0.26	0.13	0.16	0.33	13	inf occipital spheno-occipital synchondrosis left
1087	0.18	0.18	0.19	0.32	13	inf occipital spheno-occipital synchondrosis right
222	0.29	0.20	0.19	0.40	20	superior naso-maxillare left
223	0.23	0.20	0.23	0.38	20	superior naso-maxillare right
1026	0.15	0.40	0.20	0.48	19	superior orbital fissure left

Table 2.3 (cont.)

Landmark No	x	y	z	|xyz|	n	Landmark
1027	0.20	0.31	0.22	0.43	20	superior orbital fissure right
700	0.51	0.24	0.06	0.56	20	superior orbitale left
701	0.57	0.34	0.09	0.67	20	superior orbitale right
506	0.21	0.16	0.10	0.28	19	supero-lateral orbitale left
507	0.19	0.20	0.17	0.33	19	supero-lateral orbitale right
510	0.22	0.41	0.23	0.51	20	zygo-frontale left
511	0.20	0.32	0.20	0.43	20	zygo-frontale right
512	0.22	0.24	0.17	0.37	20	zygo-frontale sphenoidale left
513	0.23	0.19	0.22	0.37	20	zygo-frontale sphenoidale right
514	0.25	0.32	0.31	0.51	20	zygo-maxillare inferius left
515	0.23	0.17	0.22	0.36	20	zygo-maxillare inferius right
516	0.20	0.39	0.07	0.44	20	zygo-temporale left
517	0.38	0.35	0.16	0.55	20	zygo-temporale right

2.8.4.2 Errors of variables

For the purpose of this analysis, a total of 120 comparisons were made. They comprised 97 linear and 13 angular variables. Four variables showed significant errors at the p=0.01 level (marked with # in Table 2.4) and five had errors at the p=0.05 level (marked with * in Table 2.4).

Table 2.4 Magnitudes of errors of variables

Variable	Unit	Mean diff	Median	SD	D	t	Measurement		Description
CRANIAL VAULT									
Width	mms	N/A	N/A	N/A	0	0	cindx.l	cindx.r	Maximum cranial width
	mms	-0.1	0	0.6	0.6	-0.56	as.l	as.r	Interasterion width
	mms	0.2	0.2	0.7	0.6	1.15	po.l	po.r	Interporion width
Height	mms	0.1	0.2	0.6	0.6	0.54	ba	br	Cranial height
	mms	0	0	0.4	0.4	-0.26	br	po.l	L lateral cranial vault height
	mms	0	0.1	0.4	0.4	0.48	br	po.r	R lateral cranial vault height
	mms	0	-0.1	0.6	0.6	0.07	n	br	Anterior cranial vault height
	mms	0	0	0.8	0.8	0	l	br	Posterior cranial vault height
	mms	0.2	0.2	0.8	0.8	1.31	l	o	Lambdoid height
Length	mms	N/A	N/A	N/A	0	0	cindxa	cindxp	Maximum cranial length
	mms	-0.1	0	0.6	0.6	-0.71	spc.l	as.l	L lateral cranial vault length
	mms	-0.3	-0.2	0.6	0.6	-2.19 *	spc.r	as.r	R lateral cranial vault length
CRANIAL BASE									
Width	mms	0.5	0.2	2.1	2	1.1	spa.l	spa.r	Anterior cranial base width
	mms	0.1	0.1	0.4	0.4	1.45	ac.l	ac.r	Anterior clinoid width
	mms	-0.1	0	0.5	0.5	-0.53	petsa.l	petsa.r	Superior spheno-occipital synchondrosis width
	mms	0.1	0.1	0.3	0.3	1.34	pts.l	pts.r	Inferior spheno-occipital synchondrosis width
	mms	0.2	0.1	1.6	1.6	0.53	petp.l	petp.r	Posterior cranial fossa width
	mms	0	0	0.3	0.3	-0.22	ss.l	ss.r	External cranial base width
	mms	N/A	N/A	N/A	0	0	fmlhg.l	fmlhg.r	Foramen magnum width

Table 2.4 (cont.)

Variable	Unit	Mean diff	Median	SD	D	t	Measurement		Description
Length	mms	0.2	0	0.9	0.8	1.2	sor.l	spa.l	L anterior cranial fossa length
	mms	0.3	0.1	1	0.9	1.19	sor.r	spa.r	R anterior cranial fossa length
	mms	-0.7	-0.3	1.6	1.5	-1.95	spa.l	petp.l	L lateral middle cranial fossa length
	mms	0.4	0.4	1.2	1.2	1.25	spa.r	petp.r	R lateral middle cranial fossa length
	mms	-0.5	-0.1	1.8	1.8	-1.15	petsa.l	petp.l	L petrous ridge length
	mms	0.3	0.3	1.6	1.5	0.95	petsa.r	petp.r	R petrous ridge length
	mms	0.2	0.1	0.6	0.6	1.59	pts.l	petsa.l	L spheno-occipital synchondrosis length
	mms	-0.1	0	0.4	0.4	-0.76	pts.r	petsa.r	R spheno-occipital synchondrosis length
	mms	0.2	0.2	0.5	0.4	1.65	ba	o	Foramen magnum length
	mms	-0.1	-0.1	0.4	0.4	-1.29	ba	h	Inferior posterior cranial base length
	mms	0.1	0.1	0.3	0.3	0.68	ba	n	Cranial base length
	mms	0	0.1	0.6	0.6	0.14	ba	s	Posterior cranial base length
	mms	0	0.1	0.4	0.4	0.16	s	n	Anterior cranial base length
ORBIT									
Width	mms	-0.6	-0.6	1.1	1.1	-2.46 *	sor.l	sor.r	Anterior superior orbital width
	mms	N/A	N/A	N/A	0	0	morfl.l	morfl.r	Interorbital width
	mms	N/A	N/A	N/A	0	0	lor.l	lor.r	Maximum orbital width
	mms	-0.4	-0.6	1	1	-1.68	or.l	or.r	Anterior inferior orbital width
	mms	-0.1	-0.2	0.4	0.4	-0.77	ofa.l	ofa.r	Posterior orbital width
	mms	N/A	N/A	N/A	0	0	lor.l	morfl.l	L orbital distance
	mms	N/A	N/A	N/A	0	0	lor.r	morfl.r	R orbital distance
Height	mms	-0.1	0	0.3	0.3	-1.39	sor.l	or.l	L orbital height
	mms	0	0	0.3	0.3	-0.08	sor.r	or.r	R orbital height
Length	mms	0	0	0.5	0.4	0.29	ofa.l	sor.l	L superior orbital length
	mms	0	0	0.6	0.6	0.04	ofa.r	sor.r	R superior orbital length
	mms	-0.1	-0.1	0.4	0.4	-1.35	ofa.l	or.l	L inferior orbital length
	mms	-0.1	-0.3	0.7	0.7	-0.7	ofa.r	or.r	R inferior orbital length
	mms	N/A	N/A	N/A	0	0	ofa.l	morfl.l	L medial orbital length
	mms	N/A	N/A	N/A	0	0	ofa.r	morfl.r	R medial orbital length
	mms	0.1	0	0.5	0.5	0.55	ofa.l	slor.l	L lateral orbital length
	mms	0	-0.1	0.6	0.5	-0.37	ofa.r	slor.r	R lateral orbital length
NASAL									
Width	mms	-0.2	-0.1	0.6	0.6	-1.17	snm.l	snm.r	Superior nasal width
	mms	0.2	0.1	0.6	0.6	1.12	inm.l	inm.r	Inferior nasal width
	mms	-0.4	-0.5	0.6	0.6	-3.11 #	al.l	al.r	Nasal aperture width
Height	mms	0.1	0.1	0.5	0.5	0.75	n	al.l	L nasal height
	mms	0.3	0.2	0.7	0.6	1.65	n	al.r	R nasal height
	mms	0	0	0.3	0.3	0.26	na	ans	Nasal aperture height
	mms	-0.1	-0.1	0.5	0.5	-0.82	pns	h	Posterior nasal height
Length	mms	0.1	0.1	0.4	0.4	0.7	inm.l	snm.l	L naso-maxillary suture length
	mms	0	-0.2	0.7	0.7	0	inm.r	snm.r	R naso-maxillary suture length
	mms	0.1	0.1	0.5	0.5	0.81	na	n	Nasal bone length
MAXILLA									
Width	mms	0	0.2	0.6	0.5	-0.16	zmi.l	zmi.r	Maximum maxillary width
	mms	-0.2	-0.2	0.9	0.9	-0.91	ms.l	ms.r	Posterior superior maxillary width
	mms	0.2	0	0.7	0.7	1.26	mxt.l	mxt.r	Posterior inferior maxillary width
	mms	0	0	0.3	0.3	0.14	gpf.l	gpf.r	Posterior palatal width
Height	mms	0.2	0.1	0.5	0.5	1.76	n	ans	Anterior upper face height
	mms	0.1	0.2	0.4	0.4	0.89	ans	pr	Anterior maxillary alveolar height
	mms	-0.1	-0.1	0.5	0.5	-1.06	mxt.l	ms.l	L posterior maxillary height
	mms	0.1	-0.1	0.6	0.5	0.4	mxt.r	ms.r	R posterior maxillary height

Table 2.4 (cont.)

Variable	Unit	Mean diff	Median	SD	D	t	Measurement				Description
Length	mms	0.3	0.4	0.7	0.7	2.15 *	or.l	zmi.l			L anterior zygo-maxillary suture length
	mms	0.1	0	0.5	0.5	0.68	or.r	zmi.r			R anterior zygo-maxillary suture length
	mms	0.1	0.1	0.4	0.4	0.7	inm.l	snm.l			L naso-maxillary suture length
	mms	0	-0.2	0.7	0.7	0	inm.r	snm.r			R naso-maxillary suture length
	mms	0.1	0.1	0.4	0.4	1.07	mxt.l	pr			L inferior maxillary length
	mms	0	-0.2	0.6	0.6	-0.08	mxt.r	pr			R inferior maxillary length
	mms	0.1	0	0.3	0.3	1.08	pns	ans			Palatal length
ZYGOMA											
Height	mms	-0.1	-0.1	0.3	0.3	-0.71	slor.l	zmi.l			L zygomatic height
	mms	-0.1	-0.3	0.4	0.4	-1.55	slor.r	zmi.r			R zygomatic height
Length	mms	0.3	0.3	0.6	0.6	2.34 *	zt.l	au.l			L zygomatic arch length
	mms	0.1	0	0.6	0.6	0.89	zt.r	au.r			R zygomatic arch length
	mms	N/A	N/A	N/A	0	0	zti.l	or.l			L zygomatic length
	mms	N/A	N/A	N/A	0	0	zti.r	or.r			R zygomatic length
MANDIBLE											
Width	mms	-0.5	-0.5	0.5	0.4	-4.42 #	go.l	go.r			Intergonial width
	mms	0	0	0.2	0.2	1.04	cd.l	cd.r			Intercondylar width
	mms	0.1	0.2	0.6	0.6	0.98	cd.l	ct.l			L superior ramus distance
	mms	-0.1	-0.1	0.7	0.6	-0.99	cd.r	ct.r			R superior ramus distance
Height	mms	0.1	0	0.2	0.2	1.07	gn	id			Anterior alveolar height
	mms	-0.3	-0.4	0.7	0.6	-1.74	cd.l	go.l			L posterior ramus height
	mms	-0.2	-0.2	0.7	0.7	-1.03	cd.r	go.r			R posterior ramus height
Length	mms	0.5	0.5	0.5	0.5	3.70 #	go.l	gn			L mandibular body length
	mms	0	0.2	0.7	0.6	0.25	go.r	gn			R mandibular body length
	mms	0.1	0.1	0.4	0.4	1.14	gn	cd.l			L total mandibular length
	mms	-0.2	-0.1	0.5	0.5	-1.58	gn	cd.r			R total mandibular length
INTER-REGIONAL											
	mms	0	0	0.7	0.7	0	s	pns			
	mms	0	0	0.4	0.4	0.06	s	ans			
	mms	-0.2	-0.2	0.5	0.5	-1.8	ba	pns			
	mms	-0.1	-0.1	0.4	0.4	-1.1	ba	ans			
	mms	0.2	0.2	0.4	0.4	2.31 *	au.l	ans			L total face length
	mms	0	0.1	0.5	0.5	0.33	au.r	ans			R total face length
ANGLES											
	deg	0.1	-0.2	1.6	1.5	0.34	ba	s	n		Cranial base angle
	deg	-0.5	-0.3	1.6	1.5	-1.29	s	n	na		Nasal angle
	deg	N/A	N/A	N/A	0	0	morfl.l	n	morfl.r		Interorbital angle
	deg	-0.4	-0.3	1.1	1	-1.74	petsa.l	au.l	zt.l		L zygoma projection angle
	deg	-0.2	0	1.6	1.6	-0.55	petsa.r	au.r	zt.r		R zygoma projection angle
	deg	0	0	0.8	0.8	0.12	cd.l	go.l	gn		L gonial angle
	deg	-0.2	-0.3	0.6	0.6	-1.7	cd.r	go.r	gn		R gonial angle
	deg	-0.7	-0.6	0.7	0.7	-3.79 #	go.l	gn	go.r		Anterior mandibular angle
	deg	0.3	0.3	0.5	0.5	2.04	petp.l	es	petp.r		Petrous posterius anterior angle
	deg	-0.2	0.3	1.9	1.8	-0.36	s	n	ac.l	spa.l	L lateral projection of lesser wing
	deg	-0.5	0	1.5	1.5	-1.28	s	n	ac.r	spa.r	R lateral projection of lesser wing
	deg	0.2	0.2	1	0.9	0.99	s	n	ans	pns	Cranial base/palatal plane angle
	deg	0	-0.1	0.6	0.6	-0.25	n	ans	ans	pns	Palatal plane/face height angle

Statistically significant systematic errors at p=0.01 level were associated with measurements involving gonion on the mandible and alare on the nasal aperture. These may have resulted from the rounded nature of the gonial angle at the junction of the ramus and body of the mandible and the high variation in shape of the angle of the mandible. The same difficulties were experienced in the determination of alare point. Other landmarks that exhibited similar difficulties, with systematic errors at the p=0.05 level, were orbitale and superior orbitale on the orbital rim, auriculare at the junction of zygomatic arch and temporal bone, sphenion c and asterion on the skull.

However, the systematic errors were observed to be smaller, or of similar magnitude, to the standard deviation of the differences between determinations (Table 2.4). Those differences that exhibited statistically significant errors at the p=0.01 level were in the range of 0.4mm to 0.5mm for linear variables and 0.7^{o} for one angular variable. At the p=0.05 level of significance, the differences were in the range of 0.3mm to 0.6mm.

Average differences between determinations that were found to be statistically non-significant were in the range of 0mm to 0.7mm for linear variables and 0^{o} to 0.5^{o} for angular variables.

The random measurement errors (D) were observed to lie in the range of 0.3mm to 2.0mm for linear variables and 0.5^{o} to 1.8^{o} for angular variables (Table 2.4).

2.9 Conclusion

This chapter has shown that three-dimensional CT is an imaging technique capable of analysing the craniofacial complex comprehensively. Three-dimensional data enabled the identification and relocation of points for a large number of landmarks per subject with minimal error. All parts of the craniofacial skeleton can be quantified providing that a region has definable, reproducible landmarks. The reliability of these three-dimensional coordinate

positions opens up a valuable opportunity to study the human craniofacial complex in more detail than has been possible in the past.

It can be concluded from the error study that location of landmarks from the 3D-CT reconstructions generated in this study is both accurate and reproducible. Therefore, the approach that has been used would appear to provide a suitable means of describing the morphology of the human craniofacial skeleton in quantitative terms.

When considering the results presented in subsequent chapters, the errors of the method need to be taken into account. However, overall they were small in magnitude and unlikely to bias the results.